

Spin models from nonlinear cellular automata

Konstantinos Sfaïropoulos,* Luke Causer, Jamie F. Mair, Stephen Powell, and Juan P. Garrahan
*School of Physics and Astronomy, University of Nottingham, Nottingham, NG7 2RD, UK and
Centre for the Mathematics and Theoretical Physics of Quantum Non-Equilibrium Systems,
University of Nottingham, Nottingham, NG7 2RD, UK*

We extend the study of 1D elementary cellular automata (CA) to the nonlinear rules, following our study of the linear rules in Ref.[*arXiv:2309.08059*]. We thus construct the respective classical spin models and obtain their zero temperature ground states. We argue that these models are examples of frustrated systems where their ground state space can be exactly and systematically calculated. By including quantum fluctuations through the addition of a transverse field, we study their ground state quantum phases and phase transitions. We use rules 30, 54 and 201 as a probe of our two main results: (a) for small transverse fields we identify an order-by-disorder mechanism which stabilizes the classical phase, and (ii) we observe a first-order quantum phase transition between the classical and quantum paramagnetic phases when the transverse field strength equals the classical coupling strength, as for the linear rules.

I. INTRODUCTION

Frustration refers to the phenomenon where the degrees of freedom of a system cannot simultaneously satisfy all of their interactions [1–4]. The origin of this effect can be twofold: geometrical [5] or due to the interactions themselves [2]. A classic paradigm of geometric frustration consists of Ising spins on a triangular lattice interacting through antiferromagnetic, two-body terms. Minimization of the free energy of this classical system leads to an extensive ground state degeneracy, which was first studied by Wannier [6]. The restriction to Ising spins is in general unnecessary, since effects of frustration are equally encountered for Potts or vector spin systems [7–10].

Frustration often leads to an extensive (or subextensive) ground state degeneracy. Placing these systems under the effect of thermal or quantum fluctuations gives rise to a wealth of phenomena depending on whether the degeneracy is (fully or partially) lifted or if it persists [2]. In the former category, magnetization plateau structures might be encountered where the lifting of the degeneracy involves some kind of (spontaneous) symmetry breaking mechanism [3]. At the same time, fluctuations do not always act destructively; the stabilisation of a part of the ground state degeneracy that possesses the softest fluctuations might lead to a “fluctuation-induced” ordering or order-by-disorder (ObD) [10–14]. This ordering mechanism can be equally of thermal (thObD) or quantum (qObD) origin. A subclass of this mechanism includes the possibility of the selection of a disordered or (cooperative) paramagnetic state in what is called “disorder-by-disorder” (DbD) [15–18]. On the other hand, a cooperative paramagnet or quantum spin liquid might be formed, when the ground state degeneracy remains extensive and the spin autocorrelation functions decay exponentially (with the temperature or the distance of interactions) [19–23]. Note that the connectedness of the topology of the ground state manifold in this last case is of paramount importance [16, 24] for the existence of the spin liquid phase.

A big part of the literature has focused on the study of the

above phenomena in two paradigmatic models of condensed matter, the Heisenberg antiferromagnet [19, 20, 25] and the transverse field Ising model [15, 16, 24], placed primarily on different frustrated lattices including the triangular, with short-range [15, 26], long-range interactions [27] or in buckled colloidal monolayers [28–30], the kagome [15, 18, 24], the ruby lattice [31] or the bathroom tile [32]. Recently, these effects have been proposed to occur in systems of Rydberg atoms [33], although the quest for their experimental observation is much older [34, 35]. Ref. [34] analyzed a variety of magnetic pyrochlore oxides and the effects of frustration on them, while also reviewing another mechanism for lifting the ground state degeneracy, through the inclusion of random bonds. Similarly, spinels of the form AB_2X_4 show a number of different ordering patterns, including both an ObD and a spin liquid regime, describing diamond lattice antiferromagnets [36, 37].

The effects of fluctuations on models and materials might be drastically altered under the combined effect of quantum and thermal fluctuations. This is to be expected as the former benefit states with the smallest magnon energy, while the latter states with the largest density of low-energy excitations [38]. The interplay and the distinctive effects of quantum and thermal fluctuations, although known, has been less studied in the literature, for both Ising [39] and Heisenberg models [40–42]. In [41, 42] continuous accidental degeneracies and their respective pseudo-Goldstone modes were studied, with a qualitative signature for the detection of thOBD in materials in the latter.

Lately, frustrated models have been studied in the context of Hilbert space fragmentation and quantum many body scars, as in Ref. [43], or shown to possess disorder-free localisation [44], thus providing an avenue for connecting their study to nonthermal quantum effects [45, 46], nonequilibrium dynamics and simulations on quantum computers [47–51].

In this paper, we discuss spin models obtained from nonlinear cellular automata (CA), extending the description of the models defined in Ref. [52]. We show that these models exhibit classical frustration on the level of on-site spin operators, due to the presence of non-onsite operators and specifically controlled-Z gates. By decomposing the non-onsite operators into on-site ones, the frustration arises due to the com-

* ksfaïropoulos@gmail.com

peting interactions themselves within each classical energy term. In a similar fashion to Ref. [52], we study their classical zero-temperature ground state properties through the periodic structure of the underlying CA in the presence of periodic boundary conditions (PBC), in Sec. II, highlighting their differences from linear CA. After introducing the classical spin models in Sec. III, we then minimally couple them to a transverse field which gives rise to nontrivial quantum dynamics and study in Sec. IV their ground state quantum phase transitions.

II. INTRODUCTION TO CELLULAR AUTOMATA

Cellular automata (CA) describe a lattice of discrete cells, each hosting a degree of freedom, which in the simplest scenario is just a binary field. Generally, these states can take values from any finite field. CA describe the dynamic effect of the update of these arrays of cells with time according to a given (deterministic or probabilistic) rule [53–57].

In this work, we will concentrate on 1D elementary CA, meaning CA whose update rule is local, and is a function only of the value of the given cell and its nearest neighbors in the previous timestep. Update rules which are expressed as nonlinear functions of the values of the sites lead to some major differences compared to the CA studied previously in Refs. [52, 58].

Let us now describe these differences through the study of some specific examples. For this work, we will focus on three specific nonlinear elementary CA, Rule 30, 54 and 201. Their update rules are described in the appendix of Ref. [52], repeated here (see Fig. 1 for the convention of sites)

$$\begin{aligned} f_{30}(p, q, r) &= p + q + r + qr \\ f_{54}(p, q, r) &= p + q + r + pr \\ f_{201}(p, q, r) &= p + q + r + pr + 1, \end{aligned} \quad (1)$$

where $\{p, q, r\}$ take values 0/1 and are defined modulo 2. Note that rules 54 and 201 are complementary [57]. Example trajectories with a single nonzero initial seed for the above rules are shown in Fig. 1.

Following Ref. [52] we want to study the periodic structure of the aforementioned rules. However, the main difference compared to the linear CA is the lack of a number theoretic description [53] or, differently said, the inability to use gaussian elimination [59]. This is due to the absence of a matrix description of the update rule [53, 54]. In other words, the models (and the respective CA) studied in Refs. [52, 58] consist of XORSAT instances of constrained satisfaction problems, while the nonlinear rules here of general SAT instances.

Similarly to our previous works, the studied CA (and the corresponding spin models) exhibit a drastically different behaviour for different boundary conditions. Here, we will focus on PBC, which on the level of the CA are imposed by the space and time periodicity of the given CA.

In Fig. 2 we sketch the attractor structure for these nonlinear rules for some indicative system sizes, $N = L \times M$, while in Table I we give the cycle periods for Rule 30 up to size $L = 25$

L	C
3	1
4	8, 1
5	5, 1
6	1
7	63, 4, 1
8	40, 8, 1
9	171, 72, 1
10	15, 5, 1
11	154, 17, 1
12	102, 8, 3, 1
13	832, 260, 247, 91, 1
14	1428, 133, 112, 84, 63, 14, 4, 1
15	1455, 30, 9, 7, 5, 1
16	6016, 4144, 40, 8, 1
17	10846, 1632, 867, 306, 136, 17, 1
18	2844, 186, 171, 72, 24, 1
19	3705, 247, 133, 38, 1
20	6150, 3420, 1715, 580, 68, 30, 15, 8, 5, 1
21	2793, 597, 409, 63, 44, 42, 4, 1
22	3553, 3256, 781, 154, 77, 66, 17, 1
23	38249, 4784, 138, 1
24	185040, 5448, 366, 312, 102, 40, 20, 8, 3, 1
25	588425, 74525, 3470, 2950, 275, 5, 1

TABLE I: Periods for Rule 30.

and in Table II for Rule 54 up to $L = 35$. On contrary, Rule 201 has periods of length 2 and fixed points of length 1 of increasing number for all studied CA sizes. The number of these periods (or fixed points) increases subextensively, while always remaining bounded by the number of periodic orbits of the OBC case. For OBC the number of ground states depends on the extent of the constraint, being 2^{2L+M-2} for Rules 30, 54 and 201. For other rules where the constraint is applied to only two columns, the degeneracy is 2^{L+M-1} .

The calculation of these limit cycles for the nonlinear rules cannot be performed in an algebraic-theoretic way as for the linear ones, and one has to resort to brute-force enumeration. For this reason, we employ Floyd’s tortoise and hare algorithm [60]. Another feature of the nonlinearity concerns the lack of predictive power on the cycle lengths. For additive CA and specific sequences of system sizes, there exist techniques for the prediction of their cycle lengths. Here, we do not expect any of these techniques to apply.

III. CLASSICAL SPIN MODELS FROM NONLINEAR CA

In this section we consider the dynamical trajectories of the nonlinear one-dimensional CA as ground states of two-dimensional classical spin models, in a similar way to what we did for the linear rules in Ref. [52]. Borrowing language from quantum many-body, this correspondence allows us to define (classical) parent Hamiltonians, where the binary variables, $x_i = 0/1$, of the CA become Ising spin variables, $\sigma_i = 1 - 2x_i$, where i is a location in $(1+1)$ space-time for the CA, and in $(2D)$ space for the spin models. In this way, the nonlinear

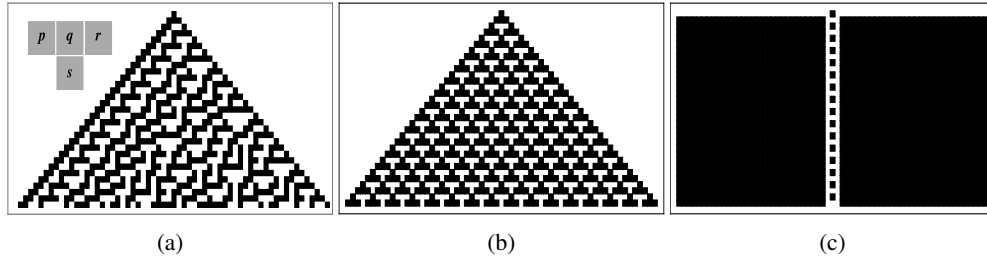


FIG. 1: CA with nonlinear rules. Evolution from a single down site for rules (a) 30 (chaotic, non-repeating pattern), (b) 54 (periodic pattern) and (c) 201 (note that this configuration starts from a single down site and immediately flips to a nearly all-down configuration). Black sites denote spin down (1) and empty sites spin up (0).

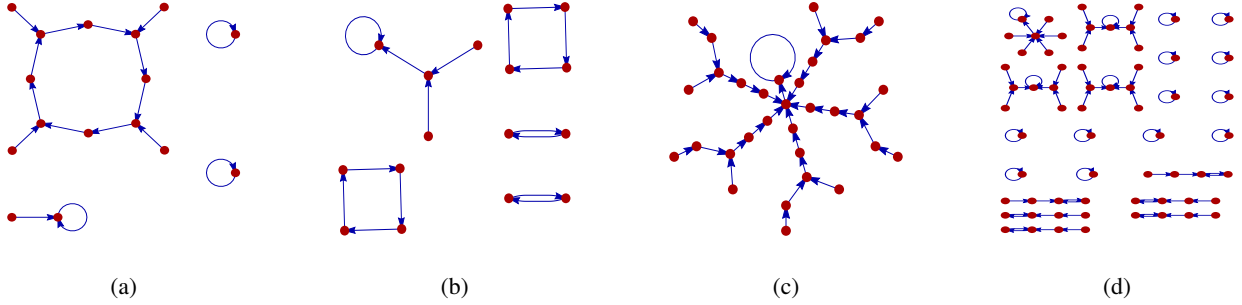


FIG. 2: The attractor and fixed point structure of (a) Rule 30 with $L = 4$, (b) Rule 54 with $L = 4$, (c) Rule 54 with $L = 5$ and (d) Rule 201 for $L = 6$. Red points represent the available states and the arrows the transitions between them, according to the given CA.

rule of a CA is mapped to an interaction between neighbouring spins, which in the language of quantum circuits are n -controlled Z (or CZ) gates: a product of two binary terms in a rule maps to a CZ gate, a three-site product to a CCZ gate and so on. For example $pq \rightarrow CZ_{pq} = (1 + \sigma_p + \sigma_q - \sigma_p \sigma_q)/2$.

The minimal 2D classical spin models whose ground states are described by the nonlinear Rules 30, 54 and 201 can be found in appendix A of Ref. [52]. More specifically, for the Rules 30 and 54 in terms of on-site and non-onsite operators we have

$$E_{30} = - \sum_{\{p,q,r,s\}} \sigma_p \sigma_q \sigma_r CZ_{qr} \sigma_s \quad (2)$$

$$E_{54} = - \sum_{\{p,q,r,s\}} \sigma_p \sigma_q \sigma_r CZ_{pr} \sigma_s, \quad (3)$$

where the sum is over all plaquette terms with sites $\{p, q, r, s\}$.

By decomposing the CZ gate, Eqs. (2) to (3) can be expressed as a sum of linear-CA terms

$$E_{30} = \frac{1}{2} (-E_{240} + E_{60} + E_{90} + E_{150}) \quad (4)$$

$$E_{54} = \frac{1}{2} (-E_{204} + E_{60} + E_{102} + E_{150}) \quad (5)$$

$$E_{201} = -E_{54}, \quad (6)$$

and by following the notation of Ref. [52] for the above clas-

sical energy terms,

$$E_{240} = - \sum_{\{p,s\} \in \setminus} \sigma_p \sigma_s \quad (7)$$

$$E_{204} = - \sum_{\{q,s\} \in \uparrow} \sigma_q \sigma_s \quad (8)$$

$$E_{60} = - \sum_{\{p,q,s\} \in \nabla} \sigma_p \sigma_q \sigma_s \quad (9)$$

$$E_{90} = - \sum_{\{p,r,s\} \in \nabla} \sigma_p \sigma_r \sigma_s \quad (10)$$

$$E_{102} = - \sum_{\{q,r,s\} \in \nabla} \sigma_q \sigma_r \sigma_s \quad (11)$$

$$E_{150} = - \sum_{\{p,q,r,s\} \in \nabla} \sigma_p \sigma_q \sigma_r \sigma_s. \quad (12)$$

The frustration due to the incompatibility of the interaction terms is apparent from the Eqs. (7) to (12). The energy function of each nonlinear rule is a sum of four terms, but the values each local interaction term takes are ± 1 . This special feature of the combinations of their couplings simplifies their respective collective result. Their combination leads to the notion of a defect, as for the linear rules, although its properties and propagation follow the nonlinear rules. Thus, these

L	C
3	1
4	4, 2, 1
5	1
6	4, 1
7	4, 1
8	8, 6, 4, 2, 1
9	27, 4, 1
10	30, 4, 1
11	99, 11, 4, 1
12	12, 10, 4, 2, 1
13	169, 4, 1
14	112, 4, 1
15	330, 4, 1
16	40, 16, 14, 8, 6, 4, 2, 1
17	289, 51, 4, 1
18	306, 90, 180, 4, 1
19	494, 437, 247, 57, 54, 27, 19, 4, 1
20	86, 60, 48, 32, 30, 24, 20, 18, 4, 2, 1
21	399, 147, 63, 14, 4, 1
22	484, 264, 242, 198, 121, 99, 32, 11, 4, 1
23	52371, 690, 575, 4, 1
24	312, 98, 56, 42, 32, 24, 22, 12, 10, 8, 6, 4, 2, 1
25	1800, 550, 115, 75, 4, 1
26	624, 546, 520, 338, 182, 169, 120, 78, 32, 26, 14, 4, 1
27	918, 837, 783, 459, 243, 81, 80, 27, 4, 1
28	224, 112, 110, 84, 64, 34, 32, 28, 26, 4, 2, 1
29	783, 725, 464, 203, 87, 80, 18, 4, 1
30	780, 750, 660, 630, 420, 330, 150, 90, 75, 32, 30, 4, 1
31	1240, 1178, 1023, 961, 651, 450, 341, 217, 93, 42, 4, 1
32	608, 544, 144, 122, 96, 72, 40, 36, 32, 30, 22, 16, 14, 8, 6, 4, 2, 1
33	1056, 1023, 957, 858, 429, 297, 143, 111, 99, 48, 11, 4, 1
34	952, 850, 816, 782, 578, 544, 289, 272, 119, 102, 51, 36, 34, 32, 4, 1
35	1540, 1470, 1225, 770, 735, 185, 105, 54, 35, 4, 1

TABLE II: Periods for Rule 54.

energy functions can be equally written as

$$\begin{aligned}
 E_{30} &= - \sum_{\{p,q,r,s\}} d_{30}(p, q, r, s) \\
 E_{54} &= - \sum_{\{p,q,r,s\}} d_{54}(p, q, r, s), \quad (13)
 \end{aligned}$$

where $d_n(p, q, r, s)$ locally constrains the N - $\{p, q, r, s\}$ quadruplets, according to the corresponding rule, cf. Fig. 1. For both linear and nonlinear CA, d_n takes values ± 1 , with -1 indicating the presence of a defect, see eg. Ref. [61, 62]. However, the specific combinations of spins and their net effect in the energy function is dictated by the CA rule.

IV. QUANTUM MODELS AND QUANTUM PHASE TRANSITIONS

In this section, we study the quantum version of these models by minimally coupling them to a transverse field,

$$H_{30/54/201} = JE_{30/54/201} - h \sum_i X_i, \quad (14)$$

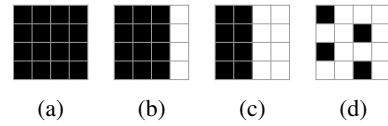


FIG. 3: The ground states for Rule 201 for a 4×4 system size. Ground states which are obtained by translations of these states are omitted

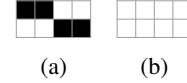


FIG. 4: Similar to Fig. 3 for the ground states of the Rule 54 for a 4×2 system size.

where in the classical energy terms we make the substitution of the Ising spins by operators, $\sigma_i \rightarrow Z_i$, where X_i and Z_i the Pauli matrices acting on site i .

Before embarking on the study of the ground state phase diagram of these models, we want to get some intuition on the effect of an infinitesimal transverse field on the classical ground state manifold of Eqs. (4-6). In Sec. IV A we also generalize this to all other spin models given by the nonlinear CA rules (in the cases where this is possible).

A. Quantum Order-by-Disorder

We first consider the nonlinear models on a case-by-case basis and for specific finite system sizes. Below we try to generalize to the thermodynamic limit (if any), and other rules, by utilizing degenerate perturbation theory [63–66].

Given a Hamiltonian, $H = H^0 + \lambda H^1$, where H^1 the perturbing potential with $\lambda \ll 1$, $H^0 |n_\mu^0\rangle = E_n^0 |n_\mu^0\rangle$, and the index μ indicating the degenerate classical ground states. The projector P projects onto the ground state manifold, so that

$$H^0 P = P H^0 = E^0 P. \quad (15)$$

We then define an effective Hamiltonian through a canonical transformation and reorder terms order by order,

$$\begin{aligned}
 H_{\text{eff}} &= e^S H e^{-S} = H + [S, H] + \frac{1}{2!} [S, [S, H]] + \dots \\
 &= H^0 + \lambda ([S^1, H^0] + H^1) + O(\lambda^2), \quad (16)
 \end{aligned}$$

where $S = \sum_{n=1}^{\infty} \lambda^n S^n$ and require that $[P, H_{\text{eff}}] = 0$ which ensures the decoupling of the ground and excited state manifolds, see [63–66]. The first and second order terms in this expansion are

$$H_{\text{eff}}^{(1)} = P H^1 P \quad (17)$$

$$H_{\text{eff}}^{(2)} = P H^1 D H^1 P, \quad (18)$$

with $D = \frac{1-P}{E^0 - H^0}$.

Let us now study the specific cases of Rules 30, 54 and 201. We start with Rule 201 and the system size 4×4 . The classical

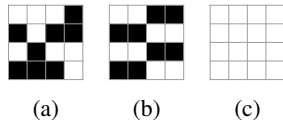


FIG. 5: Similar to Fig. 3 for the ground states of the Rule 54 for a 4×4 system size.

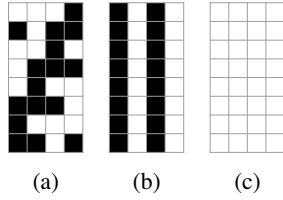


FIG. 6: Similar to Fig. 3 for the ground states of the Rule 30 for a 4×8 system size.

ground states of the model for this system size are shown in Fig. 3. An infinitesimal transverse field couples the classical ground states to second order in perturbation theory. By applying degenerate perturbation theory, we observe a splitting of the degeneracy of the classical ground states according to the number of zeros and their positions (“excited” spins, in the terminology of Rule 201). More explicitly, the corresponding matrix elements of H_{eff}^2 are sketched in Fig. 7. The first diagonal element has an energy correction $\Delta E = -4$ since each flipped spin gives rise to two excited plaquettes. For the set of states from panel (b), $3/4$ of the excited states give rise to a correction $\Delta E = -4$ while $1/4$ of them to $\Delta E = -8$. Simi-

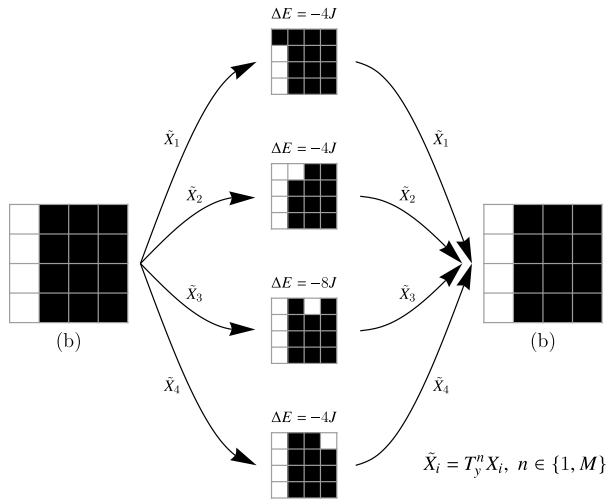


FIG. 7: A sketch of the second order processes for panel (b) of Fig. 3. Processes obtained by translating the states on the y-axis are denoted through the \tilde{X} operators, giving for each of the M processes denoted in this graph a multiplicity M .

larly for panel (c), $1/2$ to $\Delta E = -4$ and another $1/2$ of them to $\Delta E = -8$. For panel (d), $1/4$ have $\Delta E = -4$ and $3/4$ of them $\Delta E = -8$. Their energy corrections are

$$\begin{aligned} \langle (a) | H_{\text{eff},201}^{(2)} | (a) \rangle &= -\frac{Nh^2}{4J} \\ \langle (b) | H_{\text{eff},201}^{(2)} | (b) \rangle &= -\frac{3Nh^2}{4J} \frac{1}{4} - \frac{Nh^2}{4J} \frac{1}{8} = -\frac{7Nh^2}{32J} \\ \langle (c) | H_{\text{eff},201}^{(2)} | (c) \rangle &= -\frac{3Nh^2}{16J} \\ \langle (d) | H_{\text{eff},201}^{(2)} | (d) \rangle &= -\frac{5Nh^2}{32J}, \end{aligned} \quad (19)$$

respectively. All off-diagonal matrix elements of the effective Hamiltonian vanish to this order. Thus, we expect that second order degenerate perturbation theory would lead to an ordering mechanism towards the ferromagnetic (all-down) classical ground state for small transverse fields (diagonal ObD).

The same is true for any system size and ground state manifold. We thus conclude that, irrespective of the sequence of system sizes, the quantum Rule 201 will exhibit diagonal ObD for small transverse fields. This ordering mechanism does not induce any additional breaking of any symmetry of the model, since quantum fluctuations select the symmetric, ferromagnetic state.

We now consider H_{54} . A small transverse field, couples the classical ground states of a 4×2 system size to second order in degenerate perturbation theory. The ground states are shown in Fig. 4 and their energy corrections are

$$\begin{aligned} \langle (a) | H_{\text{eff},54}^{(2)} | (a) \rangle &= -\frac{3Nh^2}{16J} \\ \langle (b) | H_{\text{eff},54}^{(2)} | (b) \rangle &= -\frac{Nh^2}{8J}, \end{aligned} \quad (20)$$

respectively. In this case, the trivial ferromagnetic (all-up) ground state acquires the lowest (in absolute value) correction due to quantum fluctuations. Thus, we expect for the ground state space the selection of the state from Fig. 4(a) all the states related to it by translation symmetries. As these states are related by translations, we expect that the ground state selection would involve the spontaneous breaking of the translation symmetries (TSSB). Similarly, for larger system sizes, we expect the classical ground states with the maximum number of zeros (“unflipped” spins, in the terminology of Rule 54) to be suppressed by fluctuations. As a result, the set of states that will be favoured would be connected by translation symmetries (we expect a single fixed point in the evolution of Rule 54 for any linear system size, and thus all states from nontrivial periods would come in sets under translation symmetries), and thus TSSB in the thermodynamic limit.

For larger system sizes (and as we approach the thermodynamic limit) the second order degenerate perturbation theory might not be enough to fully resolve the degeneracy. One such case is the 4×4 system size (see Fig. 5), where the ground states involved in the two sets of states, where the states are related by translation symmetries from the two nontrivial periods, remain degenerate to second order. This degeneracy is

indeed lifted at fourth order. For larger system sizes where more nontrivial periods exist, we expect higher orders of degenerate perturbation theory to be needed. We expect that the order of the off-diagonal terms scales with (at least) the (linear) system size, while the splitting of the degeneracy on the level of the diagonal terms does not, and thus for all those cases the ground states will involve TSSB.

Finally, we discuss the situation for H_{30} . For this rule, the fixed point structure involves one fixed point for any odd linear size and 3 for any even linear size. Studying the 4×8 system size shown in Fig. 6, as for our two previous cases, the splitting occurs for second order degenerate perturbation theory with the following energy corrections (states named based on Fig. 6)

$$\begin{aligned} \langle (a) | H_{\text{eff},30}^{(2)} | (a) \rangle &= -\frac{17Nh^2}{96J} \\ \langle (b) | H_{\text{eff},30}^{(2)} | (b) \rangle &= -\frac{3Nh^2}{16J} \\ \langle (c) | H_{\text{eff},30}^{(2)} | (c) \rangle &= -\frac{Nh^2}{8J}, \end{aligned} \quad (21)$$

respectively. We observe a similar pattern of diagonal ObD with additional TSSB, as for Rule 54. However, in this case the extrapolation to larger system sizes does not clearly favour any of those states. One thing that is still clear, however, is that the mechanism for the ordering of the ground states remains the same as for both previous models studied (diagonal ObD).

As seen from the above results, there are two possible mechanisms for breaking the degeneracy: the trivial, symmetric classical ground state prevails, or a set of states connected under translational symmetries does so. These two cases differ substantially when considering perturbations of their quantum Hamiltonians with respect to their quantum phase transitions. For Rule 201, we have both small and large transverse field limits involving a trivial ground state. Thus, adding a longitudinal field perturbation for example, gives rise to paths that connect these two phases without a phase transition (since the two phases do not differ in symmetry, like what occurs with the liquid-gas transition). In contrast, for Rule 54 the presence of TSSB indicates that extra perturbations would have to cross phase boundaries to connect the two phases, which then cannot be adiabatically connected.

B. Quantum Phase Transitions

For the models studied here, we expect in a similar behaviour to that of the models in Ref. [52], with quantum phase transitions distinguishing the quantum paramagnetic phase from the classically frustrated phases. These phase transitions are expected to be of first-order with the addition of spontaneous symmetry breaking (SSB) for the cases where multiple classical ground states are encountered (cf. Ref. [52]), specifically TSSB. Below we show results from numerical simulations based on exact diagonalization [67], matrix product state (MPS) methods [68–71] (with bond dimensions up to 1000), and continuous-time quantum Monte Carlo (ctQMC) simulations [72–75] (with inverse temperature at least $\beta = 100$).

Our numerical results are shown in Figs. 8–10. For the models presented here, numerics is not as accurate as for the models from linear rules in Ref. [52]. This is most notable for the numerical MPS, probably due to the fact that the extra terms in the Hamiltonians increase the entanglement close to the phase transition point, on top of the added frustration, which has adverse effects on the convergence of the algorithm.

More precisely, Fig. 8 provides numerical evidence for the quantum phase transition for the quantum Rule 30. In all figures we use $h = 1.0$ without loss of generality. Panel (a) and (c) show the transverse magnetization per site as a function of J , $M_x = \frac{1}{N} \sum_i X_i$, for square systems $L \times L$ and PBC from numerical MPS and square and rectangular system sizes for ctQMC simulations and for rectangular stripe geometries, respectively. A gradually sharper crossover is observed at $J \approx 1.0$ which indicates the presence of a quantum phase transition in the thermodynamic limit. Panels (b) and (d) show the four-spin correlator, $M_{zzzz} = -\sum_{\{p,q,r,s\} \in \nabla} Z_p Z_q Z_r Z_s$ for square and rectangular systems from numerical MPS and ctQMC simulations, respectively. Especially in panel (b) convergence for the MPS methods deep into the frustrated phase was not always guaranteed. The jump in these observables at $J \approx 1.0$ is a clear indication of a first-order transition.

Figure 9 shows the same observables for the quantum Rule 54, whose behaviour resembles that of Rule 30. Panels (a) and (c) for square/rectangular and thin rectangular stripe geometries show clear indications of the first-order quantum phase transition, with the thin stripe ones showing a less clear discontinuity forming. MPS methods seem to struggle to converge close to the phase transition point. Similar conclusions are drawn from panels (b) and (d).

Figure 10 shows results for the quantum Rule 201. Panel (a) shows the longitudinal magnetization, $M_z = \frac{1}{N} \sum_i Z_i$, while panel (c) the transverse one. Panels (b) and (d) show the 4-spin correlator, as in Figs. 8,9. Close to the $J = 1.0$ predicted phase transition the numerics is not clear enough and convergence to the ground state is not obvious. The signatures of the quantum phase transition are confusing and the ctQMC method shows spurious effects for larger stripe geometries, when compared to the exact diagonalization data. Further numerical evidence would be needed for the clarification of the nature of the quantum phase transition close to the discontinuity point. We reason towards an enhanced hardness for the quantum Rule 201 due to the increased number of classical ground states which become low-lying excited states for the quantum model and possibly hinder the convergence of our numerical methods.

The presence of the qObD is apparent in all of these figures. More specifically, for the case of the quantum Rule 30 in Fig. 8b different system sizes seem to approach different values for the four-spin interaction magnetisation in the classical phase. This system size dependence comes from the selection of different ground states for the system sizes studied. A similar phenomenon is observed in Fig. 9(b). Lastly, in all panels of Fig. 10 we observe that the classical phase saturates the longitudinal magnetization as well as the four-spin correlator. This effect can be explained through the prism of the qObD mechanism and the selection of the symmetric, all-down fer-

romagnetic state.

Figure 11 shows the low-lying spectrum for two system sizes tractable via ED for H_{30} . In panel (b) we show the case of size 4×4 for PBC: here we show the first, second and fifth lowest energy configurations (see Table I for the correspondence of the ground state structure to the periodic orbits of the CA); the avoided crossing at $J = 1.0$ is the finite size signature of the eventual first-order transition, while the splitting away from the ground state of level 2 for $h > 1.0$ is a signature of the SSB of the symmetries. Lastly, we show the energy function as calculated from the second order perturbation theory of the previous section with solid red. In panel (c) we show the same for a system size of 3×6 where there are no limit cycles and there is only one classical minimum; here the avoided gap crossing forms between the first and the second mode. Similarly to the PBC case, the energy spectrum from ED for the lowest energy states is presented for OBC in Fig. 11a. Similar behaviour to the PBC is observed. However, the state space involved in the SSB includes many more states (2^{2L+M-2} specifically for all three models studied here) and results in hiding the avoided level crossing, which would signal the first order behaviour of the transition, behind a subextensively large low-energy spectrum. Note that there is also no ObD mechanism lifting the ground state degeneracy for OBC.

The situation becomes progressively worse for the identification of the avoided gap crossing for the quantum Rule 54 and Rule 201 in Figs. 12,13, respectively. The avoided gap crossing is easily observed for the 3×6 system size (Fig. 12c) for the quantum Rule 54, but not for the 4×4 for either OBC(Fig. 12a) or PBC(Fig. 12b). Similarly, the avoided gap crossing is harder to identify for the quantum Rule 201 for Fig. 13c and not identifiable for Fig. 13a or Fig. 13b. This is due to the many more low-lying states, close to the ground states, which give rise to the much higher classical degeneracy of the Rule 201, compared to Rules 30 or 54. It is important to note here that in Figs. 11-13 we have omitted some energy levels which do not lead to any further conclusions.

All quantum phase transitions found here are encountered for $J = h$, similar to the linear models found from CA in Refs. [52, 58]. It is tempting to extend the duality argument to the nonlinear models of this work. However, since here the defect variables mix on-site and non-onsite operators, we expect that the mapping of the terms through the standard duality procedures does not hold (see for example [76, 77]).

V. CONCLUSIONS

In this work we have analyzed the nonlinear spin models from the classification of Ref. [52] based on the 1D elementary CA. We have mapped the trajectories of the nonlinear CA to the ground states of parent spin models which consist of a sum of terms with competing classical interactions giving rise to classical frustration effects.

We have explained the differences between linear and nonlinear rules, and given that for the latter one cannot make use of the standard number theoretic tools or of Gaussian elimi-

nation, we had to resort to brute force techniques for the calculation of their periodic orbits. These in turn corresponded to the minimum energy configurations of the associated classical spin models. Making these models quantum by adding a transverse field term, we studied their corresponding ground state phase diagrams and argued that, with increasing system size, there is concrete evidence for a first-order quantum phase transition, similar to other models in this class [52, 58]. Furthermore, we have identified that the classical phases of these nonlinear models show diagonal qObD, which is distinct from what occurs for models corresponding to linear rules [52, 58], and only for PBC, something that we attribute to the presence of the non-onsite CZ gates in the definition of their classical constraints. A more complete treatment of the perturbative effects from quantum fluctuations would require the use of linked cluster expansion methods or continuous unitary transformations [78, 79].

Although clear signatures of a quantum phase transition exist, the specifics of it and its accompanying SSB (if any) could not be characterized in general terms for all our models in our numerics. We were unable to extract any meaningful information about a more general pattern for the periodic orbits or fixed points by increasing their system sizes. The only general conclusion concerns Rule 201, where we can safely argue (without a rigorous proof though) that the only periodic orbits encountered are of length 1 and 2, and that their multiplicity increases subextensively. For Rule 30 and Rule 54, the increase of the number of classical ground states is in general nonmonotonic.

The quantum phase transitions for the models we studied can be divided into two categories. One follows the paradigm of the quantum Rule 201 where the qObD leads to a trivial classical phase. The accompanying phase transition exhibits no symmetry breaking in the thermodynamic limit and resembles the one of the quantum triangular plaquette model for system sizes a power of 2 [58, 80]. The other class of models, including the quantum Rule 30 and Rule 54, show TSSB on top of the expected first order quantum phase transition in the thermodynamic limit. The two classes of models are vastly different: the first one possesses a phase transition with no symmetry change (cf. liquid-gas), while the second with a change (cf. solid-liquid).

We expect other nonlinear CA to give similar results, having similar quantum phase transitions, but also qObD. We attribute this effect to the fixed directionality of the local constraint, and to its nonlinear character. Similar models with nonlinear local constraints, such as Ref. [43, 81], but no directionality of their constraints, can in principle exhibit an exponential ground state manifold and also be candidates for spin liquid states [18]. Similarly, the constraint can be of longer support, where we would expect a similar behaviour.

In this work we focused on the zero-temperature classical properties of these models and then studied them in the presence of quantum fluctuations. However, we have not studied the effects of thermal fluctuations. We expect the occurrence of thObD for finite temperature, although a detailed study of the combination of both thermal and quantum fluctuations might reveal additional interesting phenomena [41, 42]. We

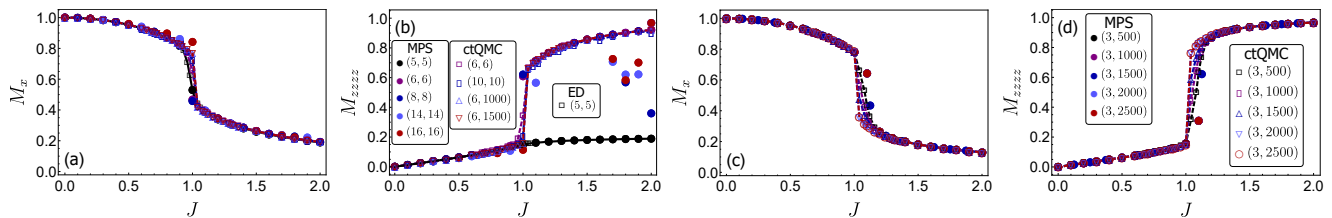


FIG. 8: **Quantum phase transition of H_{30} for PBC.** (a) Transverse magnetisation M_x as a function of J , for square system sizes $L \times L$ from numerical MPS (filled symbols) and square and rectangular sizes from ctQMC simulations (empty symbols). Exact diagonalization data shown as empty symbols and a continuous interpolating function (black). (b) Four-spin interaction magnetisation similar to (a). (c,d) Same with (a, b) for thin stripe system sizes.

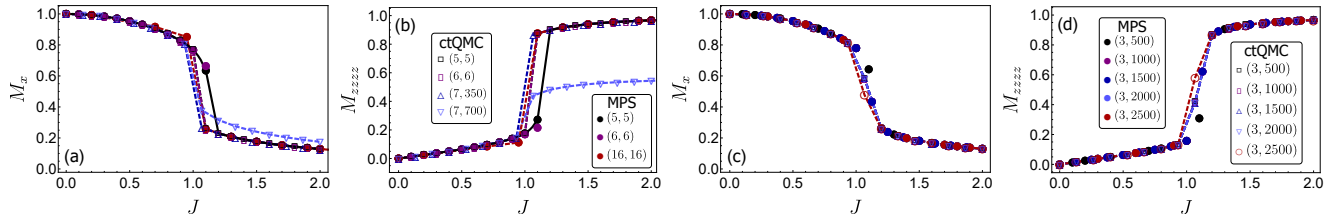


FIG. 9: **Quantum phase transition of H_{54} for PBC, similar to Fig. 8.** Exact diagonalization data in (a) and (b) are shown as a continuous (black) line.

did not study the quantum dynamics of these models either, or the possibility of any nonthermal states and a nonergodic behaviour.

ACKNOWLEDGMENTS

We acknowledge financial support from EPSRC Grants no. EP/R04421X/1 and EP/T021691/1, the Leverhulme Trust

Grant No. RPG-2018-181, and University of Nottingham grant no. FiF1/3. LC was supported by an EPSRC Doctoral prize from the University of Nottingham. Simulations were performed using the University of Nottingham Augusta and Ada HPC cluster, and the Sulis Tier 2 HPC platform hosted by the Scientific Computing Research Technology Platform at the University of Warwick (funded by EPSRC Grant EP/T022108/1 and the HPC Midlands+ consortium).

-
- [1] R. Liebmann, *Statistical Mechanics of Periodic Frustrated Ising Systems*, Lecture Notes in Physics (Springer, 1986).
- [2] H. T. Diep, *Frustrated Spin Systems*, 3rd ed. (WORLD SCIENTIFIC, 2020).
- [3] C. Lacroix, P. Mendels, and F. Mila, eds., *Introduction to Frustrated Magnetism: Materials, Experiments, Theory*, Springer Series in Solid-State Sciences, Vol. 164 (Springer, 2011).
- [4] U. Schollwöck, J. Richter, D. J. J. Farnell, and a. F. Bishop, eds., *Quantum Magnetism*, Lecture Notes in Physics (Springer, 2004).
- [5] R. Moessner and A. P. Ramirez, Geometrical frustration, *Phys. Today* **59**, 24 (2006).
- [6] G. H. Wannier, Antiferromagnetism. The Triangular Ising Net, *Phys. Rev.* **79**, 357 (1950).
- [7] A. Yoshimori, A new type of antiferromagnetic structure in the rutile type crystal, *J. Phys. Soc. J.* **14**, 807 (1959).
- [8] R. J. Elliott, Phenomenological discussion of magnetic ordering in the heavy rare-earth metals, *Phys. Rev.* **124**, 346 (1961).
- [9] T. A. Kaplan, Some effects of anisotropy on spiral spin-configurations with application to rare-earth metals, *Phys. Rev.* **124**, 329 (1961).
- [10] J. Villain, R. Bidaux, J.-P. Carton, and R. Conte, Order as an effect of disorder, *J. Physique* **41**, 1263 (1980).
- [11] C. L. Henley, Ordering by disorder: Ground-state selection in fcc vector antiferromagnets, *J. Appl. Phys.* **61**, 3962 (1987).
- [12] C. L. Henley, Ordering due to disorder in a frustrated vector antiferromagnet, *Phys. Rev. Lett.* **62**, 2056 (1989).
- [13] A. Chubukov, Order from disorder in a kagomé antiferromagnet, *Phys. Rev. Lett.* **69**, 832 (1992).
- [14] J. T. Chalker, P. C. W. Holdsworth, and E. F. Shender, Hidden order in a frustrated system: Properties of the Heisenberg Kagomé antiferromagnet, *Phys. Rev. Lett.* **68**, 855 (1992).
- [15] R. Moessner and S. L. Sondhi, Ising models of quantum frustration, *Phys. Rev. B* **63**, 224401 (2001).
- [16] R. Moessner, Magnets with strong geometric frustration, *Can. J. Phys.* **79**, 1283 (2001).
- [17] M. Powalski, K. Coester, R. Moessner, and K. P. Schmidt, Disorder by disorder and flat bands in the kagome transverse field Ising model, *Phys. Rev. B* **87**, 054404 (2013).
- [18] P. Narasimhan, S. Humeniuk, A. Roy, and V. Drouin-Touchette, Simulating the transverse-field Ising model on the kagome lattice using a programmable quantum annealer, *Phys. Rev. B* **110**, 054432 (2024).
- [19] R. Moessner and J. T. Chalker, Low-temperature properties of

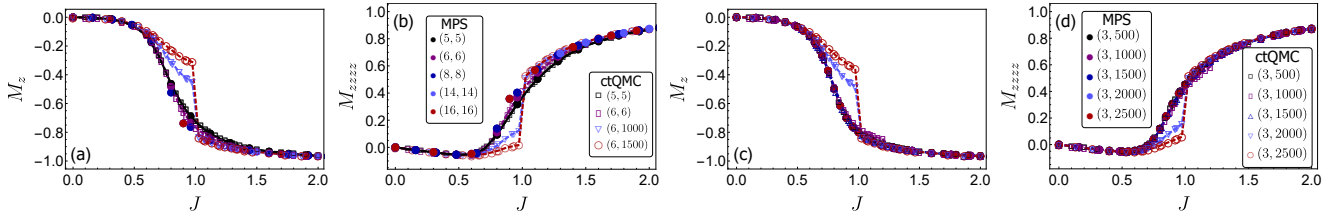


FIG. 10: Quantum phase transition of H_{201} for PBC, similar to Fig. 8. Panels (a) and (c) show the longitudinal magnetization, M_z . Exact diagonalization data as in Fig. 9.

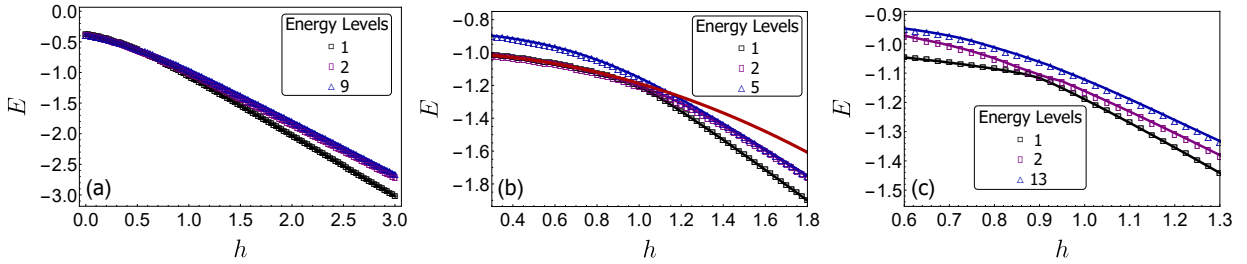


FIG. 11: Low-lying spectrum of H_{30} for a 4×4 system size with OBC (a), a 4×4 (b) and a 3×6 (c) system size for PBC for their respective modes. The avoided gap crossing is evident in panels (b) and (c). For panel (b) the solid dark red line indicates the prediction of second order degenerate perturbation theory for the ground state (E_1).

- classical geometrically frustrated antiferromagnets, *Phys. Rev. B* **58**, 12049 (1998).
- [20] R. Moessner and J. T. Chalker, Properties of a Classical Spin Liquid: The Heisenberg Pyrochlore Antiferromagnet, *Phys. Rev. Lett.* **80**, 2929 (1998).
- [21] L. Savary and L. Balents, Quantum spin liquids: a review, *Rep. Prog. Phys.* **80**, 016502 (2016).
- [22] Y. Zhou, K. Kanoda, and T.-K. Ng, Quantum spin liquid states, *Rev. Mod. Phys.* **89**, 025003 (2017).
- [23] J. Knolle and R. Moessner, A Field Guide to Spin Liquids, *Ann. Rev. Condens. Matter Phys.* **10**, 451 (2019).
- [24] R. Moessner, S. L. Sondhi, and P. Chandra, Two-Dimensional Periodic Frustrated Ising Models in a Transverse Field, *Phys. Rev. Lett.* **84**, 4457 (2000).
- [25] O. A. Starykh, Unusual ordered phases of highly frustrated magnets: a review, *Rep. Prog. Phys.* **78**, 052502 (2015).
- [26] Y. I. Dublenych, Ground states of the Ising model on an anisotropic triangular lattice: stripes and zigzags, *J. Phys.: Condens. Matter* **25**, 406003 (2013).
- [27] J. A. Koziol, M. Mühlhauser, and K. P. Schmidt, Order-by-disorder and long-range interactions in the antiferromagnetic transverse-field Ising model on the triangular lattice—A perturbative point of view, *Res. Phys.* **61**, 107794 (2024).
- [28] Y. Han, Y. Shokef, A. M. Alsayed, P. Yunker, T. C. Lubensky, and A. G. Yodh, Geometric frustration in buckled colloidal monolayers, *Nature* **456**, 898 (2008).
- [29] Y. Shokef and T. C. Lubensky, Stripes, Zigzags, and Slow Dynamics in Buckled Hard Spheres, *Phys. Rev. Lett.* **102**, 048303 (2009).
- [30] Y. Shokef, A. Souslov, and T. C. Lubensky, Order by disorder in the antiferromagnetic Ising model on an elastic triangular lattice, *Proc. Natl. Acad. Sci.* **108**, 11804 (2011).
- [31] A. Duft, J. A. Koziol, P. Adelhardt, M. Mühlhauser, and K. P. Schmidt, Order-by-disorder in the antiferromagnetic $J_1 - J_2 - J_3$ transverse-field Ising model on the ruby lattice, *Phys. Rev. Res.* **6**, 033339 (2024).
- [32] S. N. Hearth, S. C. Morampudi, and C. R. Laumann, Quantum orders in the frustrated Ising model on the bathroom tile lattice, *Phys. Rev. B* **105**, 195101 (2022).
- [33] H.-K. Wu, T. Suzuki, N. Kawashima, and W.-L. Tu, Programmable order by disorder effect and underlying phases through dipolar quantum simulators, *Phys. Rev. Res.* **6**, 023297 (2024).
- [34] J. S. Gardner, M. J. P. Gingras, and J. E. Greedan, Magnetic pyrochlore oxides, *Rev. Mod. Phys.* **82**, 53 (2010).
- [35] J. Struck, C. Ölschläger, R. L. Targat, P. Soltan-Panahi, A. Eckardt, M. Lewenstein, P. Windpassinger, and K. Sengstock, Quantum Simulation of Frustrated Classical Magnetism in Triangular Optical Lattices, *Science* **333**, 996 (2011).
- [36] D. Bergman, J. Alicea, E. Gull, S. Trebst, and L. Balents, Order-by-disorder and spiral spin-liquid in frustrated diamond-lattice antiferromagnets, *Nat. Phys.* **3**, 487 (2007).
- [37] J.-S. Bernier, M. J. Lawler, and Y. B. Kim, Quantum Order by Disorder in Frustrated Diamond Lattice Antiferromagnets, *Phys. Rev. Lett.* **101**, 047201 (2008).
- [38] R. Schick, T. Ziman, and M. E. Zhitomirsky, Quantum versus thermal fluctuations in the fcc antiferromagnet: Alternative routes to order by disorder, *Phys. Rev. B* **102**, 220405 (2020).
- [39] S. V. Isakov and R. Moessner, Interplay of quantum and thermal fluctuations in a frustrated magnet, *Phys. Rev. B* **68**, 104409 (2003).
- [40] B. Danu, G. Nambiar, and R. Ganesh, Extended degeneracy and order by disorder in the square lattice $J_1 - J_2 - J_3$ model, *Phys. Rev. B* **94**, 094438 (2016).
- [41] J. G. Rau, P. A. McClarty, and R. Moessner, Pseudo-Goldstone Gaps and Order-by-Quantum Disorder in Frustrated Magnets, *Phys. Rev. Lett.* **121**, 237201 (2018).
- [42] S. Khatua, M. J. P. Gingras, and J. G. Rau, Pseudo-Goldstone Modes and Dynamical Gap Generation from Order by Thermal Disorder, *Phys. Rev. Lett.* **130**, 266702 (2023).

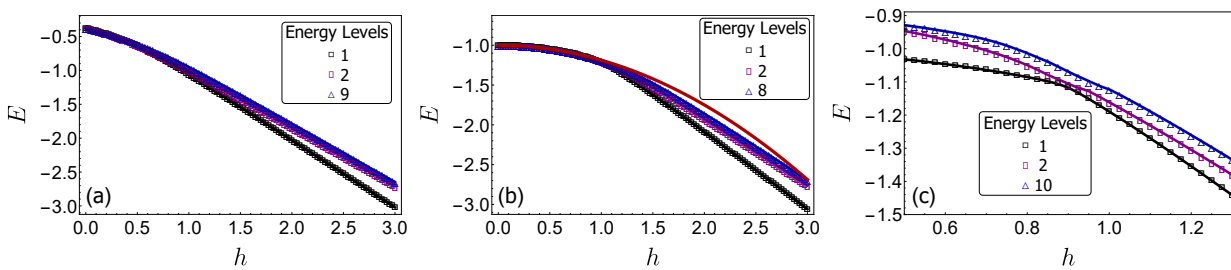


FIG. 12: **Low-lying spectrum of H_{54}** , similar to Fig. 11. The avoided gap crossing is evident only in panel (c). Similar in panel (b) the prediction of perturbation theory for the ground state included.

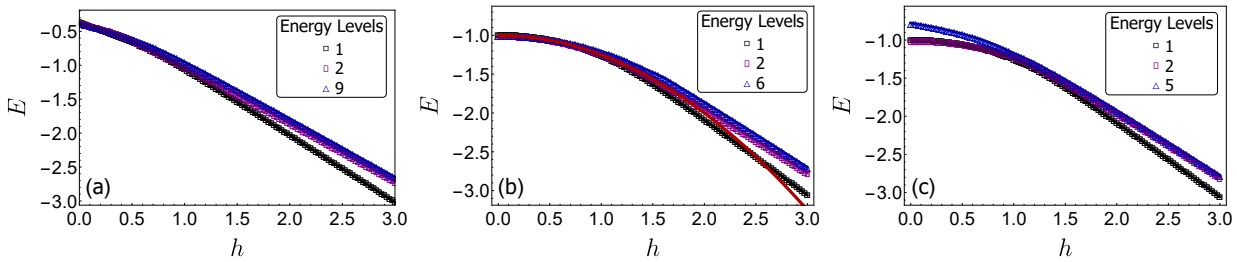


FIG. 13: **Low-lying spectrum of H_{201}** , similar to Fig. 11. The avoided gap crossing is evident only in panel (c).

- [43] D. T. Stephen, O. Hart, and R. M. Nandkishore, Ergodicity Breaking Provably Robust to Arbitrary Perturbations, *Phys. Rev. Lett.* **132**, 040401 (2024).
- [44] P. A. McClarty, M. Haque, A. Sen, and J. Richter, Disorder-free localization and many-body quantum scars from magnetic frustration, *Phys. Rev. B* **102**, 224303 (2020).
- [45] C. J. Turner, A. A. Michailidis, D. A. Abanin, M. Serbyn, and Z. Papić, Weak ergodicity breaking from quantum many-body scars, *Nat. Phys.* **14**, 745 (2018).
- [46] C. J. Turner, A. A. Michailidis, D. A. Abanin, M. Serbyn, and Z. Papić, Quantum scarred eigenstates in a Rydberg atom chain: Entanglement, breakdown of thermalization, and stability to perturbations, *Phys. Rev. B* **98**, 155134 (2018).
- [47] D. Bluvstein, A. Omran, H. Levine, A. Keesling, G. Semeghini, S. Ebadi, T. T. Wang, A. A. Michailidis, N. Maskara, W. W. Ho, S. Choi, M. Serbyn, M. Greiner, V. Vuletić, and M. D. Lukin, Controlling quantum many-body dynamics in driven Rydberg atom arrays, *Science* **371**, 1355 (2021).
- [48] S. Ebadi, T. T. Wang, H. Levine, A. Keesling, G. Semeghini, A. Omran, D. Bluvstein, R. Samajdar, H. Pichler, W. W. Ho, S. Choi, S. Sachdev, M. Greiner, V. Vuletić, and M. D. Lukin, Quantum phases of matter on a 256-atom programmable quantum simulator, *Nature* **595**, 227 (2021).
- [49] G. Semeghini, H. Levine, A. Keesling, S. Ebadi, T. T. Wang, D. Bluvstein, R. Verresen, H. Pichler, M. Kalinowski, R. Samajdar, A. Omran, S. Sachdev, A. Vishwanath, M. Greiner, V. Vuletić, and M. D. Lukin, Probing topological spin liquids on a programmable quantum simulator, *Science* **374**, 1242 (2021).
- [50] S. Ebadi, A. Keesling, M. Cain, T. T. Wang, H. Levine, D. Bluvstein, G. Semeghini, A. Omran, J.-G. Liu, R. Samajdar, X.-Z. Luo, B. Nash, X. Gao, B. Barak, E. Farhi, S. Sachdev, N. Gemelke, L. Zhou, S. Choi, H. Pichler, S.-T. Wang, M. Greiner, V. Vuletić, and M. D. Lukin, Quantum optimization of maximum independent set using Rydberg atom arrays, *Science* **376**, 1209 (2022).
- [51] D. Bluvstein, H. Levine, G. Semeghini, T. T. Wang, S. Ebadi, M. Kalinowski, A. Keesling, N. Maskara, H. Pichler, M. Greiner, V. Vuletić, and M. D. Lukin, A quantum processor based on coherent transport of entangled atom arrays, *Nature* **604**, 451 (2022).
- [52] K. Sfairopoulos, J. F. Mair, L. Causser, and J. P. Garrahan, Cellular automata in d dimensions and ground states of spin models in $(d+1)$ dimensions, *arXiv:2309.08059* (2023).
- [53] S. Wolfram, Statistical mechanics of cellular automata, *Rev. Mod. Phys.* (1983).
- [54] O. Martin, A. M. Odlyzko, and S. Wolfram, Algebraic properties of cellular automata, *Commun. Math. Phys.* **93**, 219 (1984).
- [55] P.-Y. Louis and F. R. Nardi, eds., *Probabilistic Cellular Automata: Theory, Applications and Future Perspectives*, Emergence, Complexity and Computation (Springer, 2018).
- [56] J. von Neumann and A. Taub, *Collected Works. Vol. 5: Design of Computers, Theory of Automata and Numerical Analysis* (Oxford, 1963).
- [57] S. Wolfram, *A New Kind of Science* (Wolfram Media, 2002).
- [58] K. Sfairopoulos, L. Causser, J. F. Mair, and J. P. Garrahan, Boundary conditions dependence of the phase transition in the quantum Newman-Moore model, *Phys. Rev. B* **108**, 174107 (2023).
- [59] M. Mézard and A. Montanari, *Information, Physics, and Computation* (Oxford University Press, 2009).
- [60] N. Loehr, The Tortoise and the Hare: A Factoring Fable, *Math Horizons* **29**, 18 (2022).
- [61] J. P. Garrahan and M. E. J. Newman, Glassiness and constrained dynamics of a short-range nondisordered spin model, *Phys. Rev. E* **62**, 7670 (2000).
- [62] J. P. Garrahan, Glassiness through the emergence of effective dynamical constraints in interacting systems, *J. Phys. Condens. Matter* **14**, 1571 (2002).
- [63] J. R. Schrieffer and P. A. Wolff, Relation between the Anderson and Kondo Hamiltonians, *Phys. Rev.* **149**, 491 (1966).
- [64] S. Bravyi, D. P. DiVincenzo, and D. Loss, Schrieffer-Wolff transformation for quantum many-body systems, *Ann. Phys.*

- 326, 2793 (2011).
- [65] K. Slagle and Y. B. Kim, Fracton topological order from nearest-neighbor two-spin interactions and dualities, *Phys. Rev. B* **96**, 165106 (2017).
- [66] J. J. Sakurai and J. Napolitano, *Modern Quantum Mechanics*, 3rd ed. (Cambridge University Press, 2020).
- [67] A. W. Sandvik, Computational Studies of Quantum Spin Systems, *AIP Conf. Proc.* **1297**, 135 (2010).
- [68] U. Schollwöck, The density-matrix renormalization group in the age of matrix product states, *Ann. Phys.* **326** (2011).
- [69] E. Stoudenmire and S. R. White, Studying Two-Dimensional Systems with the Density Matrix Renormalization Group, *Annu. Rev. Condens. Matt. Phys.* **3**, 111 (2012).
- [70] M. Fishman, S. R. White, and E. M. Stoudenmire, The ITensor Software Library for Tensor Network Calculations, *SciPost Phys. Codebases* , 4 (2022).
- [71] M. Fishman, S. R. White, and E. M. Stoudenmire, Codebase release 0.3 for ITensor, *SciPost Phys. Codebases* , 4 (2022).
- [72] B. B. Beard and U.-J. Wiese, Simulations of Discrete Quantum Systems in Continuous Euclidean Time, *Phys. Rev. Lett.* **77**, 5130 (1996).
- [73] F. Krzakala, A. Rosso, G. Semerjian, and F. Zamponi, Path-integral representation for quantum spin models: Application to the quantum cavity method and Monte Carlo simulations, *Phys. Rev. B* **78**, 134428 (2008).
- [74] T. Mora, A. M. Walczak, and F. Zamponi, Transition path sampling algorithm for discrete many-body systems, *Phys. Rev. E* **85** (2012).
- [75] L. Causer, K. Sfairopoulos, J. F. Mair, and J. P. Garrahan, Rejection-free quantum monte carlo in continuous time from transition path sampling, *Phys. Rev. B* **109**, 024307 (2024).
- [76] E. Cobanera, G. Ortiz, and Z. Nussinov, The bond-algebraic approach to dualities, *Adv. Phys.* **60**, 679 (2011).
- [77] P. Gorantla, S.-H. Shao, and N. Tantivasadakarn, Tensor networks for non-invertible symmetries in 3+1d and beyond, [arXiv:2406.12978](https://arxiv.org/abs/2406.12978) (2024).
- [78] J. Oitmaa, C. Hamer, and W. Zheng, *Series Expansion Methods for Strongly Interacting Lattice Models* (Cambridge University Press, 2006).
- [79] P. Adelhardt, J. A. Koziol, A. Langheld, and K. P. Schmidt, Monte Carlo Based Techniques for Quantum Magnets with Long-Range Interactions, *Entropy* **26** (2024).
- [80] L. M. Vasiloiu, T. H. E. Oakes, F. Carollo, and J. P. Garrahan, Trajectory phase transitions in noninteracting spin systems, *Phys. Rev. E* **101**, 042115 (2020).
- [81] K. Sfairopoulos and J. P. Garrahan, The quantum Newman-Moore model in a longitudinal field, [arXiv:2409.09235](https://arxiv.org/abs/2409.09235) (2024).